REVIEW

Laminar and transitional natural convection in an enclosure with complex and realistic conditions

Toru Fusegi
Heat Transfer and Fluid Dynamics, Energy Technology Research Institute, Tokyo Gas Co., Ltd., Minato, Tokyo, Japan

Jae Min Hyun
Department of Mechanical Engineering, Korea Advanced Institute of Science and Technology, Taejon, Korea

A state-of-the-art review is provided for analyses on sidewall-heated natural convection flows in an enclosure. Particular emphasis is given to those subjected to nonideal physical conditions. Delineation is made of the effects of thermal boundary conditions with substantial spatial and temporal variations. Specifically, four topical issues are considered: the finiteness of thermal conductance of the solid walls, the variable physical properties of the fluid, time-dependent thermal loading on the surface walls, and finally, the three-dimensionalities. In the present article, the main focus is placed on laminar flows in a rectangular cavity. This reveals salient flow features while disallowing distractions due to other complexities. Discrepancies between the preceding conventional two-dimensional numerical predictions with idealized boundary conditions and the available experimental measurements are highlighted. These may be attributable to the unexplored aspects of realistic flows, and parts of these are explicitly discussed here.

Keywords: natural convection in an enclosure; conducting walls; variable property effects; transient states; three-dimensional effects

Introduction

A large volume of research has been directed to natural convection in enclosures. In particular, thanks to the advent of powerful digital computers, numerical studies on the subject have attracted much attention. These shed light on various aspects of confined convective flows, such as interactions between boundary layers near the bounding walls and interior core (Ostrach 1972, 1982) and effects of the cavity aspect ratio and the inclination angle on flow patterns (Catton 1978; Hoogendoorn 1986), to name a few. A review of the more recent literature was given by Ostrach (1988). It concentrates on flows generated by differential heating at the side walls, the so-called *conventional convection*, for which the externally applied temperature gradient is perpendicular to the direction of gravitational acceleration. An article by Allard (1992) specifically addresses issues surrounding the thermal boundary conditions of thermally driven cavity flows. The major emphasis is placed on the effects of the adiabatic and completely conductive horizontal walls. Also included in the review are accounts on radiative properties of the wall and the geometrical three-dimensionalities, i.e., the end effects.

Address reprint requests to Dr. Fusegi at the Energy Technology Research Institute, Tokyo Gas Co., Ltd., 1-16-25 Shibaura, Minato, Tokyo 105, Japan.

Received 31 March 1993; accepted 13 December 1993

It is well recognized that this class of flows has important technological applications: examples include thermal insulation of buildings using air gaps, solar energy collectors and storage devices, nuclear reactor safety, furnaces and fire control in buildings, crystal growth in materials processing, and so on.

Another significant feature of the present problem is that it is mathematically well posed; the initial and boundary conditions can be specified without ambiguity. Therefore, it poses a suitable benchmark problem to test various computational techniques. For a two-dimensional (2-D) square cavity having differentially heated side walls and adiabatic horizontal surfaces, benchmark numerical solutions have been proposed in the Rayleigh number range of $10^3 \leq \mathrm{Ra} \leq 10^8$ for air (de Vahl Davis 1983; Saitoh and Hirose 1989; Hortmann et al. 1990; Le Quéré 1991). The first set of data (de Vahl Davis 1993) emerged from a comparison exercise that had attracted some 40 contributions using, chiefly, finite-difference and finite-element methods, and other approximation techniques; see de Vahl Davis and Jones (1983). These results are obtained by invoking the Boussinesq-fluid approximation and for a constant Prandtl number of 0.71. In the range of $10^4 \leq \mathrm{Ra} \leq 10^6$, more than two sets of benchmark solutions are available that have been generated using various different numerical schemes: a nonconservative second-order finite-difference method (FDM) in the stream function–vorticity formulation ($\psi - \omega$) by de Vahl Davis (1983), a nonconservative fourth-order $\psi - \omega$ FDM by Saitoh and Hirose (1989), a conservative second-order finite-volume method in the

primitive variable formulation by Hortmann et al. (1990), and a pseudo-spectral method by Le Quéré (1991). Representative physical quantities of the flow and thermal fields are compiled, which demonstrate satisfactory agreement among the data sets. To date, numerical results for high Rayleigh numbers, say, $Ra > 10^6$, are scarce. Le Quéré (1991) dealt with the well-known double-glazing problem for very high Ra, and steady-state solutions have been found to exist for Ra around 2×10^8 (Paolucci and Chenoweth 1989; Henkes and Hoogendoorn 1990). In passing, a reminder should be given that lower-order descritization schemes fail to strictly satisfy some physical requirements even if the number of nodes is increased, as pointed out by Betts and Haroutunian (1983).

From the viewpoint of practical applications of these convective flows, it is of vital importance to inquire into the extent of effects caused by imperfect, but realistic, physical conditions. Several features of special relevance to realistic systems may be, among others, nonuniform and time-dependent thermal boundary conditions at the walls, influence of variable physical properties, and the three-dimensionality of flow. In the present review article, thermally driven cavity flows are described, emphasizing the current understanding of the above-cited effects of realistic physical situations. An overview of the methodologies and physical models to deal with these conditions is provided. The existing knowledge will be illuminated in detail, and possible future research directions will be identified as a move toward performing more realistic experiments and numerical simulations of the practically relevant problems.

In order to portray the changes in field patterns caused by the deviations from idealized conditions, a simple rectangular upright cavity is selected as the flow configuration of interest. It is stressed that such a simple flow geometry contains a wealth of information. The flow data serve to examine the fundamental physics involved in natural convection in enclosures. The ensuing sections outline the currently available literature on the subject matter on an item-by-item basis: the effects of nonidealized thermal boundary conditions, variable fluid properties, transient flows, time-varying boundary conditions, and the three-dimensionality of flow.

The present review is not intended to be an up-to-date and exhaustive literature survey; rather, the primary aim is to convey to the reader a clear perspective of what has been accomplished and what remains to be investigated in order to narrow the gap between the idealized case studies and the reality of the basic flow features.

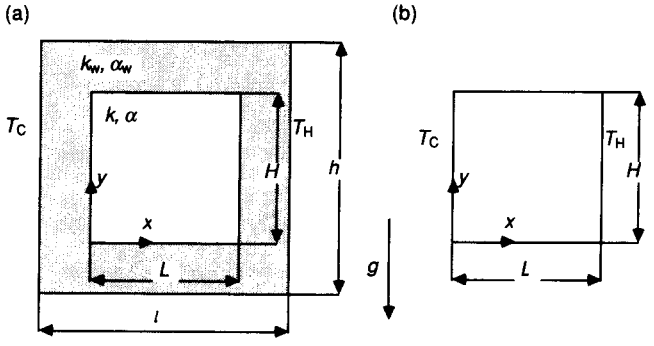

Figure 1 Schematic diagram of a differentially heated rectangular cavity. (a) Conjugate case; (b) nonconjugate case

Non-idealized thermal boundary conditions

In the standard double-glazing problem mentioned in the foregoing section, the upper and lower horizontal plates are assumed to be perfectly insulated. The entire thermal energy entering through the heated isothermal side wall reaches the opposite cooled vertical wall. For a high-aspect-ratio cavity ($A > 10$, say), the flow and heat transfer may be regarded to be one-dimensional (1-D) over much of the whole cavity height, excluding regions near the horizontal surfaces. An analytical solution can be found for quasi 1-D convection in a slot formed between two differentially heated parallel isothermal plates. Consequently, the effects of heat conduction through the horizontal surface will be more pronounced for cavities of low aspect ratios. It is easily seen that complete prevention of heat transfer across the bounding surfaces is extremely difficult in actual systems, especially when air is used as the working fluid due to its very low thermal conductivity. On the other hand, in many technological applications, it is crucial to scrutinize the thermal properties of the solid walls bounding the fluid (examples can be found in thermal insulation of a building and in solidification processes of a semiconducting material). In such cases, the convection heat transfer analysis involves a simultaneous interaction of heat conduction inside the finite-thickness solid walls and fluid motions. A schematic diagram of this conjugate problem is shown in Figure 1a. The conventional natural convection inside a cavity (Figure 1b) may be treated as a limiting case in which the wall thickness is very

Notation

A	Aspect ratio, H/L
g	Gravitational acceleration
H	Cavity height
$\mathbf{i}$	Unit vector (0, 1, 0)
k	Thermal conductivity
L	Cavity width
p	Nondimensional pressure, $(p' - p_\infty)(L/\alpha)^2/\rho$ where p_∞ is hydrostatic pressure
Ra	Rayleigh number, $g\beta(T_H - T_C)L^3/\alpha\nu$
T	Nondimensional temperature, $(T' - T_C)/(T_H - T_C)$
T_C, T_H	Cooled and heated isothermal sidewall temperatures, respectively
T_e	Environmental temperature
$\mathbf{V}$	Nondimensional velocity vector, $\mathbf{V}'(L/\alpha)^2$
W	Cavity depth

Greek symbols

α	Thermal diffusivity
β	Volumetric thermal expansion coefficient
ν	Kinematic viscosity
ρ	Density
τ	Nondimensional time, $\tau'\alpha/L^2$
∇	Gradient operator

Subscript

w	Solid wall

Superscript

	Dimensional value

thin. The pertinent governing equations for the fluid region under the usual Boussinesq approximation are

$$\nabla \cdot \mathbf{V} = 0 \tag{1}$$

$$\partial \mathbf{V}/\partial \tau + \mathbf{V} \cdot \nabla \mathbf{V} = -\nabla p + \mathrm{Pr}\nabla^2 \mathbf{V} + \mathrm{RaPr}T\mathbf{i} \tag{2}$$

$$\partial T/\partial \tau + \mathbf{V} \cdot \nabla T = \nabla^2 T \tag{3}$$

Supplementing the above equations, a heat-conduction equation for the solid region, with a constant isotropic thermal diffusivity and in the absence of internal heat generation, is the well-known Poisson equation:

$$\nabla^2 T = 0 \tag{4}$$

At the solid–fluid interface ($x = 0$, L and $y = 0, H$), the temperature and heat flux must be continuous. The latter requirement is mathematically expressed as

$$\left(\frac{\partial T}{\partial n}\right)_{\text{fluid}} = \frac{k_w}{k}\left(\frac{\partial T}{\partial n}\right)_{\text{wall}} \tag{5}$$

where n is the coordinate normal to the interface. This problem formulation is complete when the boundary conditions at the upper and lower part of the external wall surfaces are prescribed, together with appropriate initial conditions for transient problems.

A combined experimental and computational study was carried out by Kim and Viskanta (1984) for an air-filled cavity formed inside a solid block, having the void fraction ϕ defined as L^2/l^2 in the range of $0.25 < \phi < 0.6$. A comparison of measured and computationally predicted temperature distributions for the fluid region is depicted in Figure 2. For the specific case considered, a modified Rayleigh number, Ra*,

$$\mathrm{Ra}^* = \frac{g\beta(T_h - T_C)L^4}{\nu\alpha l} \tag{6}$$

is set equal to 1.01×10^6, and the thermal conductivity and diffusivity ratios of the solid wall material and the fluid are, respectively, 7.4 and 0.008. The effects of the finite-conductance walls are evident in the results. The surface temperature of the connecting horizontal boundaries varies in a nonlinear fashion, in contrast to a linear temperature profile obtainable for the case of perfectly conducting walls. The value of Ra is relatively high, but thermal stratification in the interior core region has not been well established. It should be noted that the temperature inversion is conspicuous near the lower-left and upper-right corners of the cavity. This creates the local

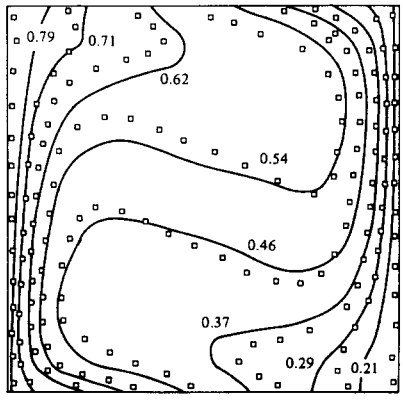

Figure 2 Comparison of the measured (symbol) and predicted (line) steady-state temperatures for air at $\mathrm{Ra}^* = 1.01 \times 10^6$ (Kim and Viskanta 1984). The left side wall is heated. The figures indicate temperature values

"heated-from-bottom" situation, which destabilizes the flow at higher Rayleigh numbers (Henkes and Hoogendoorn 1990). The experimental data points acquired from spatially averaged (in the spanwise direction) 2-D interferometric fringe patterns and the computed isotherm contours based on the 2-D calculations are qualitatively consistent. The overall Nusselt number at the vertical side wall of the cavity has been obtained as a three-parameter empirical correlation (Kim and Viskanta 1984):

$$\overline{\mathrm{Nu}} = 0.410\,\phi^{0.93}\,(k_w/k)^{0.138}\mathrm{Ra}^{*0.2} \tag{7}$$

for $10^5 < \mathrm{Ra}^* < 10^7$, $0.3 < \mathrm{Pr} < 50$, $0.25 < \phi < 0.6$, and $3 < k_w/k < 100$. This correlation can be compared with the existing formulae for the conventional nonconjugate problem (Figure 1b),

$$\overline{\mathrm{Nu}} = \begin{cases} 0.13\mathrm{Ra}^{0.28} & \text{(completely conducting)} \\ 0.138\mathrm{Rs}^{0.30} & \text{(perfectly insulated)} \end{cases} \tag{8}$$

due to Roux et al. (1978) in the range $10^4 < \mathrm{Ra} < 10^5$. In the above, the boundary conditions for the horizontal walls are either completely conducting or perfectly insulated. An explicit quantitative comparison is not possible owing to the difference in the definitions of the Rayleigh numbers used.

The thermal characteristics in the fluid as well as in the solid for a tall cavity with finite-thickness walls ($A = 10$) were numerically investigated by Kasarhérou and Le Quéré (1989). It is well known that sidewall-heated natural convection, in general, exhibits oscillatory behavior when the critical Rayleigh number, Ra_{cr}, is exceeded. It follows that the determination of Ra_{cr} constitutes an important task in the convection studies. The available data (e.g., Paolucci and Chenoweth 1989; Henkes and Hoogendoorn 1990) point to the fact that there is a difference of approximately two orders of magnitude in the value of Ra_{cr}, depending on whether the horizontal walls are completely conducting or perfectly insulated. The critical Rayleigh number for the conducting horizontal walls is smaller than that for insulated walls, due to the presence of the unstable thermal stratification that is attainable when the horizontal walls are completely conducting. A literature review for these two extreme cases is documented elsewhere (Papanicolaou and Jaluria 1992). Three distinctively different mechanisms have been proposed for the causes of flow instability, depending on the thermal conditions of the horizontal walls: the Rayleigh–Bénard instability, which is applicable to the conducting-wall case; the internal hydraulic jump at the adjoining corners where the sidewall boundary layers impinge; and the Tollmien–Schlichting traveling wave instability taking place inside the vertical boundary layers. Considerable research has endeavored to clarify the nature of these instabilities, which are believed to be an early stage of the transition towards turbulence (Papanicolaou and Jaluria 1992).

The numerical study of Kasarhérou and Le Quéré (1989) attempted to reveal the effects of wall conduction inside the vertical walls on the characteristics of oscillatory motions. The idealized horizontal walls ($h = H$) are assumed to be adiabatic. At $\mathrm{Ra} = 2.8 \times 10^8$, which is slightly above the critical Rayleigh number for the insulated horizontal wall, the thermal coupling is found to reduce the oscillation amplitude appreciably. However, the value of Ra_{cr} remains unchanged. Since this problem can find applications in materials processing and in nuclear reactor safety analyses, it is of interest to examine the effects of conduction of the bounding horizontal walls.

On the side of computational modeling, solutions of a conjugate heat transfer problem require more calculations, since the conduction inside the solid regions has to be resolved

as well. Although some novel numerical treatments have been suggested, e.g., as harmonic mean conductivity of fluid and solid to deal with conjugate problems (Patankar 1980), a straightforward extension of a solution procedure for the flow field could be wasteful. Therefore, it is a logical step to devise a simple, yet sufficiently accurate, physical model to calculate the heat conduction in the solid walls.

Recall the continuity constraint for the interfacial heat flux (Equation 5). If it is possible to assume 1-D conduction inside the solid, the constraint may be reduced to

$$\left(\frac{\partial T}{\partial x}\right)_{\text{fluid}} = \frac{k_w}{k}\frac{T_e - T}{t} \tag{9}$$

where $t = l - L$ and T_e denotes the temperature of the environment. The parameter $(k_w/k)/t$ has the physical dimension of m^{-1}, and it is referred to as the thermal conductance (Rahm and Walin 1979). The major attractiveness of this simplified model lies in the fact that one does not actually have to solve the heat conduction equation in the solid. The effects of the solid-wall heat conduction are incorporated by way of the boundary condition; hence, a substantial saving of computer time is possible.

The accuracy of this model was examined in Kaminski and Prakash (1986); they compared computed results for the full-conjugate case (2-D model) with those of the above simplified treatment (1-D model). Both models were tested to a conjugate problem involving a square cavity with a heated finite-thickness side wall. The cooled wall and adiabatic horizontal plates were presumed to be very thin. The local heat flux distribution at the solid–fluid interface for $Ra = 0.7 \times 10^6$ is plotted for various elevations in Figure 3. Computed results also include the predictions using the lumped parameter approach, in which the total heat transfer rate across the interface is estimated based on the assumption that the interface temperature is uniform. As can be seen, the difference between 1-D and 2-D models is negligibly small, while the oversimplified lumped parameter approach can produce a reasonable prediction only in an averaged sense.

Three-dimensional (3-D) simulations of natural convection in a box were performed by Le Pentrec and Lauriat (1990). They adopted the simple heat conduction model of Rahm and Walin. The above-mentioned 1-D thermal conductance model is applied to the two end plates ($z = 0, W$). Radiation effects were accounted for in terms of a correction factor for the thermal conductance. Air and water were considered as the media filling the cavity. The variations in the absolute values of the average Nusselt number at the isothermal side wall for various cavity aspect ratios (depth/width, A_z) are displayed in

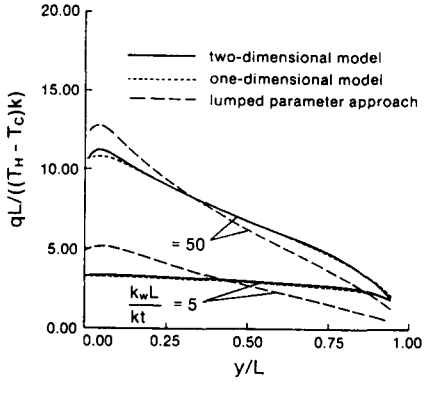

Figure 3 Comparison of the local heat flux at the solid–fluid interface predicted by different conduction models for $Ra = 0.7 \times 10^6$ (Kaminski and Prakash 1986)

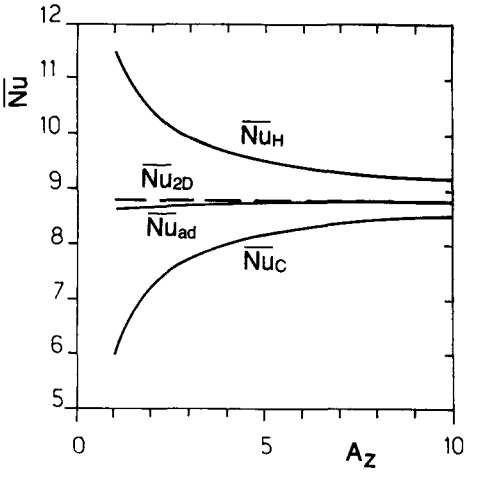

Figure 4 Variations of the absolute value of the heat transfer rate at the isothermal walls versus the depth aspect ratio for an air-filled enclosure at $Ra = 10^6$, $k_wL/kt = 11.5$ (with radiation correction), and $T_e = T_C$ (Le Pentrec and Lauriat 1990). $\overline{Nu}_C$ and $\overline{Nu}_H$, at the cooled and heated walls, respectively; $\overline{Nu}_{ad}$, with adiabatic end walls; $\overline{Nu}_{2D}$, 2-D results

Figure 4. The temperature of the environment, T_e, is set equal to the cooled isothermal wall temperature. The discrepancy between the heat transfer rates for the heated wall ($\overline{Nu}_H$) and cooled wall ($\overline{Nu}_C$) is attributed to the heat transfer across the end walls, since the horizontal walls are adiabatic. The results indicate that, if A_z is larger than 10 for an air-filled cavity, the end effects are very small. They find that the end effects in the case of water as the working fluid are far less significant; only $A_z = 2$ will suffice to suppress satisfactorily the 3-D effects. For an air-filled cubical container, Fusegi et al. (1993) show the effects of heat conduction at the horizontal and end walls as well as the effects of the environmental temperature, T_e, by using the thermal conductance model. Due to the small depth-to-width ratio ($A_z = 1$), the three-dimensionality is evident. These computational works demonstrate the robustness of the thermal conductance approach. They assumed constant values of thermal conductances; however, it could be even more useful if the thermal conductances are allowed to have proper spatial variations for modeling actual physical phenomena more faithfully.

The variable-property effects

In the majority of numerical studies for natural convection flows, the Boussinesq approximation is customarily invoked. For incompressible flows, the computational advantage is evident when one closely examines the calculation procedure of the equation of state to determine the density field. An explicit step is needed to compute density when working with a non-Boussinesq fluid. The Boussinesq approximation bypasses the task of density evaluation; the temperature computed from the energy equation is directly substituted into the buoyancy term of the momentum equation.

The necessary prerequisite to justify the use of the Boussinesq approximation is that the overall temperature difference should be sufficiently small. Quantitative assessments of this point have been performed as to natural convection in a differentially heated square cavity by Zhong et al. (1985). The main conclusion was that, when the overall temperature difference $\delta(=(T_H - T_C)/T_C)$ is less than 0.1, the Boussinesq approximation yields adequate predictions of the flow field. A somewhat wider

margin for δ may be allowed to compute the average heat transfer rate. The computations of Zhong et al. (1985) suggested that reasonably accurate values of average heat transfer rates could be obtained by using the Boussinesq approximation for up to $\delta \cong 0.2$.

The mathematical formulation for a variable-property fluid is understandably far more complex. The complete governing equations are available in, e.g., Leonardi and Reizes (1981). Their steady-state results for sidewall-heated cavities (with $A = 1$ and 2) illustrate asymmetric field patterns, which are caused by the temperature dependence of the fluid properties. Both the viscosity and thermal conductivity were assumed to be temperature dependent in their study.

Hyun and Lee (1989) demonstrated that in the transient process of heat-up, the variable viscosities modeled in an exponential form caused the heat inflow to the cavity to exceed the heat outflow. Hence, the cavity acted as a receiver of net heat input until the energy balance was reached at the steady state. This situation would not occur for the constant-viscosity case, since the idealized field patterns will exhibit exact symmetry about the vertical centerline.

The stability of a variable-property fluid flow has been extensively investigated by the numerical work of Chenoweth and Paolucci (1986). The flow-regime diagram is constructed in Figure 5. The parameter ε, denoting the overall temperature difference, is defined as $(T_H - T_C)/(T_H + T_C)$. Air is considered as the medium for which the variations of the viscosity and thermal conductivity are assumed to obey the Sutherland law. It can be seen that the critical Rayleigh number for variable-property fluids is, in general, lower than that of the Boussinesq fluid.

Transient processes

In the context of the present review, the transient phenomena of natural convection in cavities may be classified into two categories. The first refers to the time-evolving process in an approach to the large-time state. The second occurs when the external boundary conditions are prescribed in a time-dependent manner. The large-time behavior may be characterized by a stationary state consisting of a sequence of periodic phenomena. Although these transient processes are important in many thermal engineering and modern technological innovations, studies on transient (time-varying) natural convection have received far less attention.

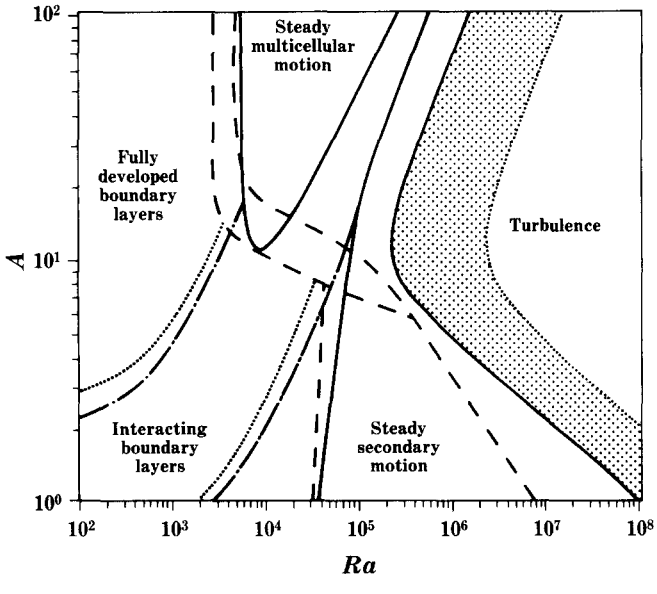

Figure 5 Dependence of the flow regions on A, Ra, and ε (Chenoweth and Paolucci 1986). For —— and —·—, $\varepsilon \ll 1$; for – – – – and ·····, $\varepsilon = 0.6$. Shaded area denotes transition to turbulence for $\varepsilon \ll 1$

Patterson and Imberger (1980), in a classical treatise, addressed the fundamental mechanisms involved in the transient behavior of natural convection in a 2-D rectangular cavity. Their analysis centered on the flow of an initially isothermal fluid, driven by abruptly raising and lowering the respective vertical sidewall temperatures of the rectangle. Relying heavily on scaling arguments and physical insight, Patterson and Imberger provided broad classifications of the transient flow regimes in terms of several nondimensional parameters. A key contention that emerged from their analysis was the existence of a decaying oscillatory approach to steady state; they stated that this behavior reflected the result of a transient system-scale internal wave activity. It was demonstrated that the criterion for such oscillatory behavior was

$$\mathrm{Ra} > \mathrm{Pr}^4 A^{-4} \tag{10}$$

Patterson and Imberger presented a few illustrative numerical solutions for a square cavity, and their results were shown to be compatible with their theoretical expositions.

The presence of the internal gravity waves in transient cavity convection has been a topic of intense discussion in the recent literature. The issue of the internal gravity waves does not appear to have been completely resolved for the flow configuration of Patterson and Imberger (1980). Laboratory measurements (Yewell et al. 1982) employing shallow cavities ($A = 0.0625$ and 0.0112) showed no evidence of waves, pointing to an apparent discrepancy between theory and experiment. Later, Patterson (1984) proposed more detailed orderings for the regime classifications, and asserted that the experiments by Yewell et al. were actually performed in a regime in which internal wave activity would not be expected. Ivey (1984) conducted similar experiments in a water-filled square cavity at Rayleigh numbers of the order of 10^9, which were much higher than the values ($\mathrm{Ra} \sim 10^5$) used in the numerical computations of Patterson and Imberger (1980). The results did not, however, give conclusive evidence of the regular internal wave oscillations expected; however, there were indications of a much higher-frequency signal that appeared to be associated with the downstream behavior of the horizontal intrusions from the corners. This was interpreted by Ivey as an internal hydraulic jump.

Transient-flow visualization and thermal-field visualization were undertaken by Lee and Kauh (1984) for a square cavity filled with water ($\mathrm{Pr} = 5.9$) for $10^5 < \mathrm{Ra} < 10^8$. This parameter range falls within the regime classification for which the presence of internal waves is expected. Figure 6 reproduces a series of photographs showing evolutions of transient fields at $\mathrm{Ra} = 2.5 \times 10^7$. The locations of the temperature front are clearly discernible in the interferograms. A noteworthy feature is an overshoot of the temperature front as it intrudes into near the mid-height of the boundary layer at the opposite side wall (Figure 6 (10)) and then moves backward slightly (Figure 6 (12)). This behavior was observed only once in the entire transient process, and clear signs of oscillatory activities were not detected in their measurements. Based on an estimation of the internal Froude number, it appeared that an internal hydraulic jump was present near the corner of the cavity. Note that the Rayleigh number range of Lee and Kauh's (1984) experiments was much lower than that considered in Ivey (1984).

The properties of these intrusions and the associated high-frequency waves have been debated in numerical studies

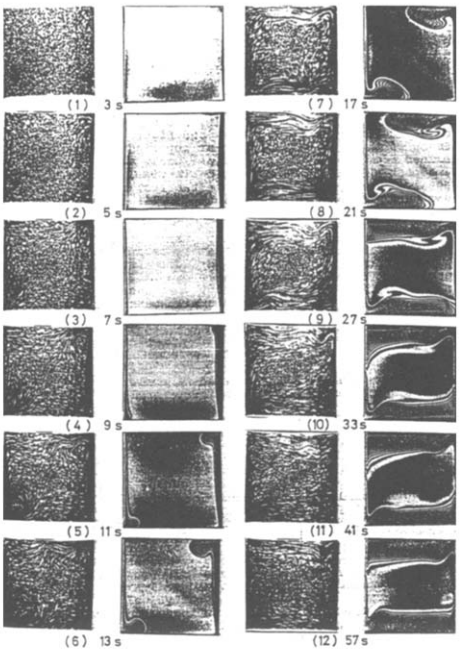

Figure 6 Flow and temperature fields visualization results for $Ra = 2.5 \times 10^7$ and $Pr = 5.9$ (Lee and Kauh 1984)

by Paolucci and Chenoweth (1989), Schladow et al. (1989), Schladow (1990), and Armfield and Patterson (1991). A combined numerical and experimental investigation (Patterson and Armfield 1990) examined the apparent conflict between the numerical and existing experimental results with respect to the oscillatory approach to steady state. They identified the principal features of the flow development, and a description of the associated generation mechanisms was offered for $Ra = 3.26 \times 10^8$, $Pr = 7.5$, and $A = 1$. This experimental condition falls within the regime boundaries proposed by Patterson and Imberger (1980) for which clear oscillatory behavior is anticipated. Their conclusions were that the scaling arguments given in Patterson and Imberger were verified, and that the high-frequency signals observed experimentally by Ivey (1984) and numerically (Paolucci and Chenoweth 1989; Schladow 1990) were thought to be sorts of instabilities. Hyun and Lee (1989) also conducted a numerical study on the existence of internal wave oscillations over broad ranges of both Ra and Pr. When $Pr > 1$, a distinct oscillatory behavior occurred if $Ra \geq Pr^4 A^{-4}$. The period of oscillations was comparable to the period of internal gravity waves. These were in support of the flow-regime classifications of Patterson and Imberger. When $Pr < 1$, an oscillatory approach to the steady state is detected only when Ra is sufficiently high to render a strong boundary-layer-type flow. Using mixtures of glycerol and water to enable wide variations of Pr, Jeevaraj and Patterson (1992) acquired measurements encompassing several flow regimes of Patterson and Imberger. Their results were also consistent with the flow-regime classifications.

Full-scale and reduced-scale model experiments were conducted using a shallow rectangular enclosure with aspect ratio of 1/3 at Ra_H (based on the room height H) of approximately 10^{10} (Olson and Glicksman 1991). The transient processes to steady-state convective flow patterns, which started from two distinctively different initial conditions, were investigated. An air-filled cavity was constructed for the full-scale test, while a refrigerant was used for the scale-model experiments. This seems to be the only available transient measurement using air. The first case dealt with the standard transient problem; namely, the flow was initially motionless, and all the walls were at a constant temperature. The temperatures of one or both side walls were instantaneously raised or lowered. In another type of transient test, the pre-existing steady-state flow was disturbed by a differential sidewall heating. Measurements were made of the process of the return to the steady state after the disturbance was removed. The mechanical disturbance was provided by stirring the flow by operating ceiling vanes. Based on smoke-flow visualizations using a scale model, Olson and Glicksman observed that the characteristic length of the flow could be scaled with the distance that the flow traveled up the vertical wall and through a horizontal loop, i.e., $H + 2L$. Defining a buoyancy convection velocity $V_0 = (g\beta(T_H - T_m)H)^{1/2}$, where T_m is the mean fluid temperature, Olson and Glicksman proposed a convection time constant to scale the time of convection-dominated flow processes. The time constant τ_{conv} was chosen to be

$$\tau_{conv} = (H + 2L)/V_0 \tag{11}$$

They showed that for the evolution of flow from a quiescent state, the initial transient phase lasted for approximately 30 nondimensional time units (τ'/τ_{conv}). In this phase, the temperature in the upper half of the core region increased. This was accomplished by formation of the circulation near the ceiling when one side wall was suddenly heated. Temperatures in the lower core region increased at a slower rate due to the horizontal boundary-layer entrainment. This is illustrated in Figure 7, which depicts the vertical temperature profiles. It was further stated that τ_{conv} was the proper measure to characterize the return to steady state in the case of the imposed mechanical disturbance.

When the thermal boundary conditions at the cavity walls vary continuously in time, time-dependent natural convection flow ensues. Of particular interest would be the cases in which the thermal boundary conditions undergo periodic changes. Specific applications of these situations are abundant. In electronic equipment cooling, electric components are energized intermittently in a periodic manner. Another example may be found in building heat transfer; the building is exposed to variations in the ambient conditions and air-conditioning systems. The daily changes of these external conditions can be approximately modeled by periodic fluctuations.

The response of the flow in a tall vertical cavity ($A = 3$), subjected to periodic surface temperature variations of the side

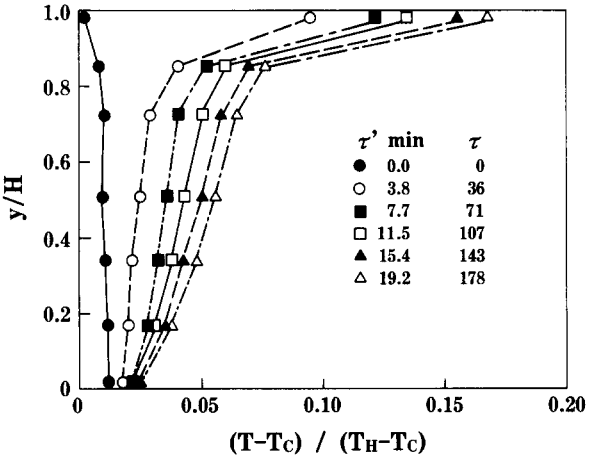

Figure 7 Vertical temperature profiles at $x/L = 0.5$ for transient heating with no cooling for the scale model (Olson and Glicksman 1991)

walls, was studied analytically and numerically by Yang et al. (1989). The side wall temperature at $x = L$ varies as a sinusoidal function:

$$T = \sin(2\pi f \tau) \tag{12}$$

where f is a dimensionless frequency. The opposite side wall ($x = 0$) also experiences a sinusoidal temperature change, but with a phase lag of π radians. The primary objective of this investigation was the validation of a numerical technique by comparing the predictions with those of a closed-form analytic solution for a cavity with very high aspect ratio. Assuming adiabatic horizontal walls, the finite-difference numerical solutions were obtained for $10^1 \leq \mathrm{Ra} \leq 10^6$ and $\mathrm{Pr} = 7.0$. Figure 8 displays the heat-transfer rate Q and the phase shift θ_3 as functions of Ra. The amplitude of the heat transfer rate increases with Ra due to the pronounced convection effects. As to the phase shift, it attains an almost constant value that is close to $\pi/4$ for low and moderate Ra; it drops off sharply as the flow bears the boundary-layer character $\mathrm{Ra} > 10^5$).

Natural convection in a square cavity, when the heated side wall has a sinusoidal temperature fluctuation, was numerically studied by Kazmierczak and Chinoda (1992). The effects of amplitude and period of the temperature variations are examined for fixed Ra and Pr, $\mathrm{Ra} = 1.4 \times 10^5$ and $\mathrm{Pr} = 7$. It is demonstrated that a secondary flow cell of smaller size appears periodically in response to the fluctuations of the surface temperature. This effect is seen near the cavity upper-left corner where the heated-wall boundary layer impinges on the ceiling. Although the heat transfer rate at the heated wall fluctuates in a periodic manner, the surface temperature variation exerts insignificant effects on the Nusselt number at the cooled side wall, which does not deviate much from the value of nonoscillatory wall temperature.

The flow parameter ranges are far extended in a numerical and theoretical investigation by Lage and Bejan (1993); namely, $10^3 \leq \mathrm{Ra}_q \leq 10^9$ and $0.01 \leq \mathrm{Pr} \leq 7$, where Ra_q is a modified Rayleigh number based on the uniform heat flux q'' imposed to the heated side wall, $\mathrm{Ra}_q = g\beta q''_m H^4/\alpha\nu k$, q''_m being the mean value of the heat flux. Instead of the sinusoidal temperature variation, a pulsating heat input is assigned at the heated wall. A novel feature of the flow is resonance characterized by maximum fluctuations in the total heat transfer rate through the vertical midplane of the cavity. The heat transfer enhancement due to the resonance is seen to be pronounced as Ra increases.

There appears to be no reported experimental work on natural convection with time-varying boundary conditions. It is believed that the difficulties are formidable in realizing well-controlled thermal boundary conditions in the experiment.

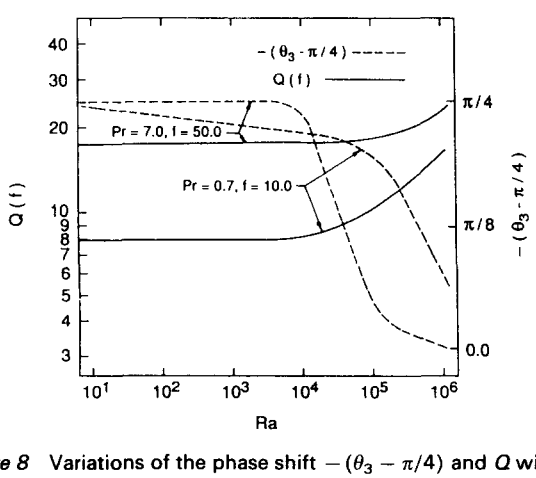

Figure 8 Variations of the phase shift $-(\theta_3 - \pi/4)$ and Q with Ra (Yang et al. 1989)

Three-dimensional effects

Most prior numerical and experimental investigations have been restricted to 2-D situations. For computational studies, this situation was unavoidable in view of the limited capability of the conventional mainframe machines and the prohibitively high cost for computing 3-D flows. Needless to say, in order to move closer to the practical systems, 3-D computations are highly desirable. However, due to the constraint of available computational resources, full-scale 3-D simulations are still in an infant stage. Earlier 3-D numerical solutions (e.g., Ozoe et al. 1976; Mallinson and de Vahl Davis 1977) have illustrated rudimentary flow structures in a rectangular box. The steady-state 3-D streamlines exhibit double-helical patterns and significant transverse flows. These endeavors are limited to low Rayleigh numbers. Consequently, the sidewall boundary layers and a nearly stagnant interior-core structure were not distinctively discernible. The case of $\mathrm{Ra} = 10^6$ was studied by Lee et al. (1988). The qualitative features of double-helical structure remained unchanged, although the inner helix had its center inside one of the two secondary vortices formed near a side wall.

The presence of the end walls in an actual enclosure exerts 3-D effects, particularly in the regions close to the walls. The secondary corner vortices, with their axes normal to the x–z plane, were found in the region adjoining the vertical lines formed by the side and end walls in $\mathrm{Ra} \geq 10^6$ (Lankhorst and Hoogendoorn 1988). The magnitude of these secondary eddies is much smaller than that of the primary roll cell, the axis of which is perpendicular to the x–y plane. Obviously, the existence of such a 3-D flow structure could not be predicted under the 2-D assumption.

An experimental and computational study was reported for a long enclosure having a square cross section and a depth aspect ratio (W/L) of 2.72 (Weaver and Viskanta 1990). Nitrogen was the working fluid. Flow visualization, using smoke and Mach–Zehnder interferometric temperature measurements, was undertaken for two values: $\mathrm{Ra} = 1.34 \times 10^5$ and $\mathrm{Ra} = 6.24 \times 10^5$. The results clearly demonstrate the existence of 3-D fluid motions in the z-direction. The qualitative features of the flow field are in accord with the numerical predictions. However, as to the quantitative assessment of the temperature distribution in the midsymmetry plane ($z = W/2$), discrepancies between the measured and calculated profiles are pronounced as the side walls are approached. It should be noted that these two sets of data could not be compared directly, since the experimentally obtained temperature distribution has been spatially averaged and the axial (z-directional) variations of the temperature field are not resolved precisely.

Hiller et al. (1989) experimentally examined 3-D flows in a cubic enclosure for high Prandtl number fluids ($200 < \mathrm{Pr} < 7000$) composed of mixtures of glycerol and water. The flow structure is described with a topological interpretation of the singularities in the flow, such as foci, nodes, and saddle points. Experiments were performed to observe the transition from one-roll (unicellular flow) and two-roll systems. The transition between these flow patterns is a continuous process as Ra is gradually raised. Subsequently, an experimental and numerical effort was made (Hiller et al. 1990). The study documented unresolved discrepancies between the computations and experiments in the value of the critical Ra at which the spiral patterns were observed in the enclosure. As to the causes,

conduction from the uninsulated walls or highly temperature-dependent fluid property variations was listed.

For more quantitative assessments of the 3-D flow characteristics, the previous numerical investigations do not have proper spatial resolutions. Furthermore, they were restricted to steady-state results.

A series of comprehensive 3-D calculations has been recently performed (Fusegi et al. 1991a, 1991b, 1992, 1993) with a view toward delineating 3-D cavity flows inside an air-filled cubical box. Relying heavily on the vector-processing supercomputers, spatial resolutions of these 3-D solutions are refined to a level comparable to those achieved in previous high-accuracy 2-D computations. The majority of the results were generated for the cases of the thermally insulated horizontal and end walls, although conducting walls were also considered.

Figure 9 represents the profiles of the Nusselt number at an isothermal side wall averaged over each z-station ($\overline{\mathrm{Nu}}(z)$). For $\mathrm{Ra} \leq 10^5$, $\overline{\mathrm{Nu}}(z)$ increases monotonically as the symmetry plane ($z = 0.5$) is approached. In contrast, at $\mathrm{Ra} = 10^6$, two minor peaks appear at around $z = 0.2$ and 0.8, due to the presence of intense convective flows in the z-direction. The overall Nusselt number, $\mathrm{Nu}_{\mathrm{overall}}$ ($= \int_0^1 \overline{\mathrm{Nu}}(z)\, dz$), and $\overline{\mathrm{Nu}}(z)_{2\mathrm{D}}$ for a 2-D enclosure (regarded as $\mathrm{Nu}_{\mathrm{overall}}$ for 2-D situations) are also plotted in the same figure. The difference between $\mathrm{Nu}_{\mathrm{overall}}$ and $\overline{\mathrm{Nu}}(z)_{2\mathrm{D}}$ gradually decreases as Ra is raised. This is explained by the fact that at higher Ra, the 3-D variations in $\overline{\mathrm{Nu}}(z)$ are confined into a narrower region close to the end walls, and $\overline{\mathrm{Nu}}(z)$ in the remaining portion is almost uniform. The difference between the numerical values of $\overline{\mathrm{Nu}}(z)$ at the midsymmetry plane ($z = 0.5$) and $\overline{\mathrm{Nu}}(z)_{2\mathrm{D}}$ is seen to be minor for the Ra range investigated, indicating that the 2-D assumption can provide a good first estimate for this cubical cavity. However, this would not be necessarily valid if different thermal boundary conditions are assigned at the end walls. Note that the end walls are assumed to be perfectly insulated in the above investigation.

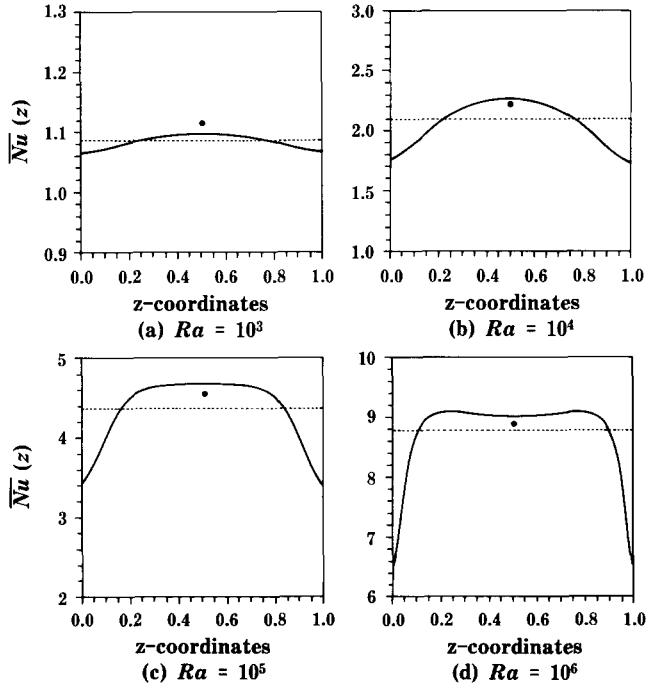

Figure 9 Distributions of the mean Nusselt number in the z-direction for $10^3 \leq \mathrm{Ra} \leq 10^6$ (Fusegi et al. 1991a). ——, $\overline{\mathrm{Nu}}(z)$ (3-D); ·····, $\mathrm{Nu}_{\mathrm{overall}}$; •, $\overline{\mathrm{Nu}}(z)_{2\mathrm{D}}$

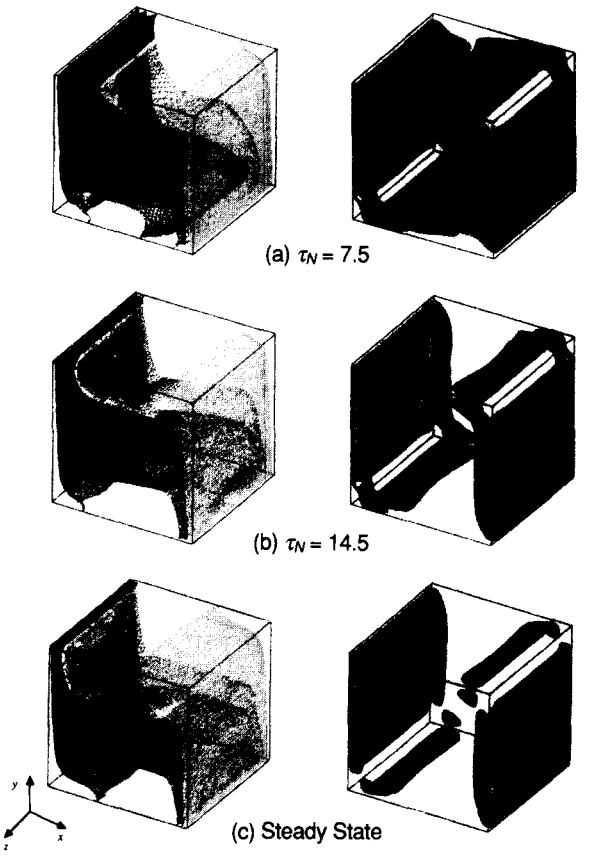

Figure 10 Evolution of the temperature field (left) and flow field (right) for transient natural convection in air at $\mathrm{Ra} = 10^6$ (Fusegi et al. 1991b). Contour increments: 1/6 for temperature, and 3.6 for vorticity. (a) $\tau_N = 7.5$; (b) $\tau_N = 14.5$; (c) steady state

The time evolutions of the temperature and flow fields for a heat-up process at $\mathrm{Ra} = 10^6$ were examined numerically by Fusegi et al. (1991b). Perspective views of the fields are displayed in Figure 10. Initially, the fluid is at a uniform temperature and motionless. A sudden differential heating at $\tau \geq 0$ at the two vertical side walls ($x = 0$ and 1) creates sharp temperature gradients in the proximity of the isothermal walls. In the central region of the enclosure, the fluid is still at the initial uniform temperature; thus, the heated fluid near the side wall at $x = 1$ starts to rise, and the cooled fluid near $x = 0$ moves downward. Subsequent to this initial development, the heated and cooled fluids flow along the ceiling and floor of the enclosure, respectively, in the opposite directions. After some time, these flows meet each other near the corners of the horizontal walls. The flow field at this stage is sketched in Figure 10a. Near the end walls ($z = 0$ and 1), the isotherms adjacent to the horizontal walls ($y = 0$ and 1) develop appreciable z-variations. This is due to the no-slip conditions imposed at the end walls. Consequently, vorticity is generated in these wall regions.

After the fluid layers merge, a piling up of the fluid in the corner areas between the side walls and horizontal walls takes place, as expounded by Patterson and Imberger (1980) for 2-D situations. This increases the overall temperature gradients in the vicinity of the isothermal walls. In the interior regions, the thermal field begins to stratify, as demonstrated in Figure 10b. The vorticity field illustrates that intense flow is now mostly confined into thin layers in the proximity of the vertical isothermal walls, in conjunction with the formation of the stratified structure in the interior.

As time progresses, the thermal stratification is substantially accomplished, with the resulting near-stagnant interior core. As the steady state is approached (see Figure 10c), the global field is characterized by a combined structure of the boundary layers near the walls and the almost-stagnant interior core. It would be worth noting that the three-dimensionality of the fields is discernible, especially in the early transient stage of the flow.

In accordance with the regime classification of Patterson and Imberger (1980) for a 2-D cavity, the flow condition ($Ra = 10^6$, $Pr = 0.71$, and $A = 1$) satisfies the previously cited criterion (Equation 10) for the presence of internal waves. The period of oscillation for the 2-D case is given as

$$\tau_N = 2\pi(1 + A^2)^{1/2} \tag{13}$$

where $\tau_N = \tau' N$, N being the Brunt–Väisälä frequency:

$$N = [g\beta(T_H - T_C)/L]^{1/2} \tag{14}$$

As depicted in Figure 11, oscillatory behavior is conspicuous in the computed results of time history of the overall Nusselt number at the midplane of the isothermal side walls located at $x = 0.5$. The oscillation period is found to be approximately 12.0, which is consistent with the 2-D analytical estimate. The oscillations in Figure 11 decay after a few cycles due to the effects of viscosity, leaving some uncertainties in determining the exact value of the period based on the computed results.

In an insightful experimental investigation, Briggs and Jones (1985) employed a nearly cubic enclosure with completely conducting horizontal walls. They demonstrated that the steady-state flow ceased to exist when Ra slightly exceeded 10^6. Beyond the critical Ra, regular steady periodic oscillations appeared in the field, the frequency of which took discrete values as Ra was raised. Since the publication of this pioneering study, much work has been done on the analytical and computational front to identify the nature of the instability. For a 2-D square cavity, Henkes and Hoogendoorn (1990) attributed the onset of instability to the Rayleigh–Bénard type arising near the horizontal boundaries due to the presence of temperature inversion. Based on a linear stability analysis of the 2-D steady-state equations, Winters (1987) demonstrated that the onset of the oscillatory convection occurred as Hopf bifurcation. The prediction Ra_{cr} was shown to be in good agreement with the measured value of Briggs and Jones (1985).

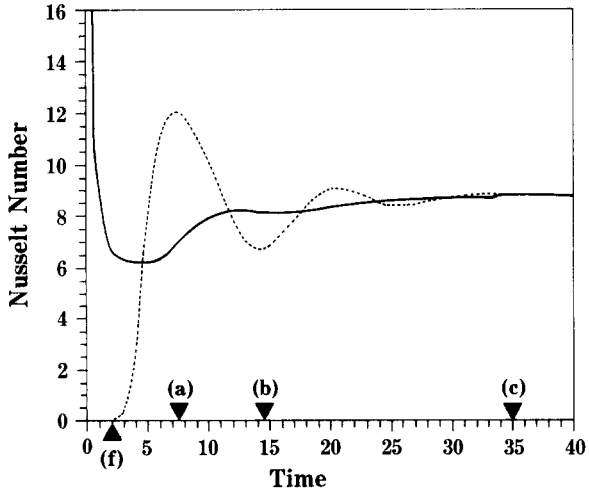

Figure 11 Evolution of the overall Nusselt number for transient natural convection in air at $Ra = 10^6$ (Fusegi et al. 1991b). The time instances correspond to those shown in Figure 10; ——, at the heated wall ($x = 1$); ·····, in the midplane ($x = 0.5$)

In a supplementary account of their experimental investigation, Jones and Briggs (1989) performed 2-D calculations for certain exemplary cases to gain insight into the local characteristics of the fields. They reported that the measured horizontal centerline velocity profiles at $Ra = 9 \times 10^6$ were nearly 20% larger than the 2-D numerical results. As to the vertical wall centerline velocity, experimental and calculated values differed no more than 3%. The onset of oscillations was about $Ra = 3 \times 10^6$ in the experiment; however, the computational predictions, including those conducted independently (Le Quéré and Alziary de Roquefort 1986; Winters 1987; Henkes and Hoogendoorn 1990), were found to be consistently lower, at around $Ra = 2.1 \times 10^6$. Jones and Briggs (1989) ascribed these discrepancies to the undetected three-dimensionalities of flow present in an actual experimental setup.

These conjectures could only be substantiated by performing 3-D investigations. Fusegi et al. (1992) carried out a full 3-D computation for a cubic cavity at $Ra = 8.5 \times 10^6$. The results exhibited that the bulk of the flow field could be thought to be nearly 2-D. This is probably due to the imposition of transverse-uniform temperature condition at the horizontal boundary walls. An inspection of the centerline velocity profiles at the symmetry plane ($z = 0.5$) is revealing. The agreement between the 3-D numerical results and the experimental data of Briggs and Jones (1985) is satisfactory. It is recalled that the previous 2-D computations of Jones and Briggs (1989) produced equally consistent results.

Computed results of a more recent high-resolution calculation (Janssen et al. 1993) indicate that the mechanism of instability in a 3-D cavity is of 2-D nature. An estimated critical Rayleigh number is approximately 2.3×10^6, which is only a 10% increase compared to the previous 2-D predictions.

A critical area that needs significant improvements is numerical visualization techniques for computed 3-D results. Since the field is 3-D in nature, proper and accurate interpretations of numerical data may be greatly aided by elaborate 3-D computer graphics capabilities.

An isolevel contour map for, e.g., temperature, and a velocity vector plot, which is the standard representation tool of the 2-D field structure, is not suitable for effectively conveying 3-D information. Perspective views of the 3-D fields, such as those shown in Figure 10, may serve better to gain overall pictures of the fields. (It should be remarked that in the original figures, each isolevel surface is represented by a different color.) Stereographic presentations of 3-D flows have been attempted in Pepper (1987); stereographic films and videotapes would be natural extensions of this technique, and they can enhance the understanding of complex 3-D flow fields.

For 3-D calculations, postprocessing of voluminous numerical data is as important as the process of obtaining solutions, and it is definitely one of the areas in which much progress is expected.

Concluding remarks

As briefly outlined in the preceding sections, an appreciable body of knowledge has been accumulated regarding the principal characteristics of a geometrically simple enclosure, particularly for 2-D situations. The state of the nonidealized boundary walls exerts a measurable impact on the field features well into the cavity interior. Consequently, experimenters should exercise proper care to have good control over the thermal boundary conditions, particularly when working with air, since certain of the idealized conditions used in computations are virtually unrealizable. The variable-property effects can cause substantial deviations from the idealized

behavior under the Boussinesq approximation. An experimental verification is warranted, together with theoretical considerations, for the adequacy of the Boussinesq approximation in a high Ra range.

Transient flow characteristics have not been explored in sufficient detail. Various aspects of the dynamics prominent in the transient state have been touched upon; however, they are still far from a stage of comprehensive understanding of this technologically important subfield of research.

Owing to the advent of high-performance supercomputing, engineering 3-D computations become increasingly feasible. Quantitative evaluations of numerical results may now be conducted on the local flow variables. As stated earlier, in order to have maximum utilization of the numerical data, a great deal of work is called for to devise effective data reduction and presentation methods.

Acknowledgment

We are grateful to an anonymous referee for pointing out additional references.

References

Allard, F. 1992. Effects of thermal boundary conditions on natural convection in thermally driven cavities. *Turbulent Natural Convection in Enclosures, A Computational and Experimental Benchmark Study*, R. A. W. M. Henkes and C. J. Hoogendoorn (Eds.), Editions Européennes Thermigue et Industrie, Paris, pp. 234–256.

Armfield, S. W. and Patterson, J. C. 1991. Direct simulation of wave interactions in unsteady natural convection in a cavity. *Int. J. Heat Mass Transfer*, **34**, 924–940

Betts, P. C. and Haroutunian, V. 1983. A stream function finite element solution for two-dimensional natural convection with accurate representation of Nusselt number variation near a corner. *Int. J. Numer. Meth. Fluids*, **3**, 605–622

Briggs, D. G. and Jones, D. N. 1985. Two-dimensional periodic natural convection in a rectangular enclosure of aspect ratio one. *J. Heat Transfer*, **107**, 850–854

Catton, I. 1978. Natural convection in enclosures. *Proc. 6th Int. Heat Transfer Conf.*, **6**, 13–31

Chenoweth, D. R. and Paolucci, S. 1986. Natural convection in an enclosed vertical air layer with large horizontal temperature difference. *J. Fluid Mech.*, **169**, 173–210

de Vahl Davis, G. 1983. Natural convection of air in a square cavity: a bench mark numerical solution. *Int. J. Numer. Meth. Fluids*, **3**, 249–264

de Vahl Davis, G. and Jones, I. P. 1983. Natural convection in a square cavity: a comparison exercise. *Int. J. Numer. Meth. Fluids*, **3**, 227–248

Fusegi, T., Hyun, J. M., Kuwahara, K., and Farouk, B. 1991a. A numerical study of three-dimensional natural convection in a differentially heated cubical enclosure. *Int. J. Heat Mass Transfer*, **34**, 1543–1557

Fusegi, T., Hyun, J. M., and Kuwahara, K. 1991b. Transient three-dimensional natural convection in a differentially heated cubical enclosure. *Int. J. Heat Mass Transfer*, **34**, 1559–1564

Fusegi, T., Hyun, J. M., and Kuwahara, K. 1992. Three-dimensional numerical simulation of periodic natural convection in a differentially heated cubical enclosure. *Appl. Sci. Res.*, **49**, 271–282

Fusegi, T., Hyun, J. M., and Kuwahara, K. 1993. Three-dimensional natural convection in a cubical enclosure with walls of finite conductance. *Int. J. Heat Mass Transfer*, **36**, 1993–1997

Henkes, R. A. W. M. and Hoogendoorn, C. J. 1990. On the stability of the natural convective flow in a square cavity heated from the side. *Appl. Sci. Res.*, **47**, 195–220

Hiller, W. J., Koch, S., and Kowalewski, T. A. 1989. Three-dimensional structures in laminar natural convection in a cubic enclosure. *Exp. Thermal Fluid Sci.*, **2**, 34–44

Hiller, W. J., Koch, S., Kowalewski, T. A., de Vahl Davis, G., and Behnia, M. 1990. Experimental and numerical investigation of natural convection in a cube with two heated side walls. *Proc. IUTAM Symp. Topolog. Fluid Mech.* Cambridge University Press, Cambridge, UK, pp. 717–726

Hoogendoorn, C. J. 1986. Natural convection in enclosures. *Proc. 8th Int. Heat Transfer Conf.*, **1**, 111–120

Hortmann, M., Peric, M., and Scheuerer, G. 1990. Finite volume multigrid prediction of laminar natural convection: bench-mark solutions. *Int. J. Numer. Meth. Fluids*, **11**, 189–207

Hyun, J. M. and Lee, J. W. 1988. Transient natural convection in a square cavity of a fluid with temperature-dependent viscosity. *Int. J. Heat Fluid Flow*, **9**, 278–285

Hyun, J. M. and Lee, J. W. 1989. Numerical solutions for transient natural convection in a square cavity with different sidewall temperatures. *Int. J. Heat Fluid Flow*, **10**, 146–151

Ivey, G. N. 1984. Experiments on transient natural convection in a cavity. *J. Fluid Mech.*, **144**, 389–401

Janssen, R. J. A., Henkes, R. A. W. M., and Hoogendoorn, C. J. 1993. Transition to time-periodicity of a natural-convection flow in a 2D differentially heated cavity. *Int. J. Heat Mass Transfer*, **36**, 2927–2940

Jeevaraj, C. G. and Patterson, J. C. 1992. Experimental study of transient natural convection of glycerol-water mixtures in a side heated cavity. *Int. J. Heat Mass Transfer*, **35**, 1573–1587

Jones, D. N. and Briggs, D. G. 1989. Periodic two-dimensional cavity flow: effect of linear horizontal thermal boundary condition. *J. Heat Transfer*, **111**, 86–91

Kaminski, D. A. and Prakash, C. 1986. Conjugate natural convection in a square cavity: effect of conduction in one of the vertical walls. *Int. J. Heat Mass Transfer*, **29**, 1979–1988

Kasarhérou, J. and Le Quéré, P. 1989. Influence of wall conduction on the transition to unsteady natural convection in a tall air-filled cavity. *Proc. 6th Int. Conf. Numer. Meth. Thermal Prob.*, Part 1, Pineridge, Swansea, UK, pp. 534–544

Kazmierczak, M. and Chinoda, Z. 1992. Buoyancy-driven flow in an enclosure with time periodic conditions. *Int. J. Heat Mass Transfer*, **35**, 1507–1518

Kim, D. M. and Viskanta, R. 1984. Study of the effects of wall conductance on natural convection in differentially oriented square cavities. *J. Fluid Mech.*, **144**, 153–176

Lage, J. L. and Bejan, A. 1993. The resonance of natural convection in an enclosure heated periodically from the side. *Int. J. Heat Mass Transfer*, **36**, 2027–2038

Lankhorst, A. M. and Hoogendoorn, C. J. 1988. Three-dimensional numerical calculations of high Rayleigh number natural convective flows in enclosed cavities. *Proc. 1988 Nat. Heat Transfer Conf., ASME-HTD 96*, **3**, 463–470

Le Pentrec, Y. and Lauriat, G. 1990. Effects of the heat transfer at the side walls on natural convection in cavities. *J. Heat Transfer*, **112**, 370–378

Le Quéré, P. 1991. Accurate solutions to the square thermally driven cavity at high Rayleigh number. *Comput. Fluids*, **20**, 29–41

Le Quéré, P. and Alziary de Roquefort, T. 1986. Transition to unsteady natural convection of air in vertical differentially heated cavities: influence of thermal boundary conditions on the horizontal walls. *Proc. 8th Int. Heat Transfer Conf.*, **4**, 1533–1538

Lee, T. S. and Kauh, S. 1984. Unsteady natural convection in a rectangular enclosure. *Proc. Korea–U.S. Semin. Thermal Eng. High Technol.* Hemisphere, Washington, pp. 51–63

Lee, T. S., Son, G. H., and Lee, J. S. 1988. Numerical predictions of three-dimensional natural convection in a box. *Proc. 1st KSME-JSME Thermal Fluids Eng. Conf.*, **2**, 278–283

Leonardi, E. and Reizes, J. A. 1981. Convective flows in closed cavities with variable fluid properties. *Numerical Methods in Heat Transfer*, R. W. Lewis et al. (Eds.). John Wiley, New York, pp. 387–412

Mallinson, G. D. and de Vahl Davis, G. 1977. Three-dimensional natural convection in a box: a numerical study. *J. Fluid Mech.*, **83**, 1–31

Olson, D. A. and Glicksman, L. R. 1991. Transient natural convection in enclosures at high Rayleigh number. *J. Heat Transfer*, **113**, 635–642

Ostrach, S. 1972. Natural convection in enclosures. *Advances in Heat Transfer* (Vol. 8). Academic Press, New York, 161–227

Ostrach, S. 1982. Natural convection heat transfer in cavities and cells. *Proc. 7th Int. Heat Transfer Conf.*, **1**, 365–379

Ostrach, S. 1988. Natural convection in enclosures. *J. Heat Transfer*, **110**, 175–1190

Ozoe, H., Yamamoto, K., Churchill, S. W., and Sayama, H. 1976. Three-dimensional numerical analysis of laminar natural convection in a confined fluid heated from below. *J. Heat Transfer*, **98**, 202–207

Paolucci, S. and Chenoweth, D. R. 1989. Transition to chaos in a differentially heated vertical cavity. *J. Fluid Mech.*, **201**, 379–410

Papanicolaou, E. and Jaluria, Y. 1992. Transition to a periodic regime in mixed convection in a square cavity. *J. Fluid Mech.*, **239**, 489–509

Patankar, S. V. 1980. *Numerical Heat Transfer and Fluid Flow*. Hemisphere, Washington, p. 45

Patterson, J. C. 1984. On the existence of an oscillatory approach to steady natural convection in cavities. *J. Heat Transfer*, **106**, 104–108

Patterson, J. C. and Armfield, S. W. 1990. Transient features of natural convection in a cavity. *J. Fluid Mech.*, **219**, 469–497

Patterson, J. and Imberger, J. 1980. Unsteady natural convection in a rectangular cavity. *J. Fluid Mech.*, **100**, 65–86

Pepper, D. W. 1987. Modeling of three-dimensional natural convection with a time-split finite-element technique. *Numer. Heat Transfer*, **11**, 31–55

Rahm, L. and Walin, G. 1979. On thermal convection in stratified fluids. *Geophys. Astrophys. Fluid Dynamics*, **13**, 51–65

Roux, B., Grodin, J. C., Bontoux, P., and Gilly, B. 1978. On a high-order accurate method for the numerical study of natural convection in a vertical square cavity. *Numer. Heat Transfer*, **1**, 331–349

Saitoh, T. and Hirose, K. 1989. High-accuracy bench mark solutions to natural convection in a square cavity. *Comput. Mech.*, **4**, 417–427

Schladow, S. G. 1990. Oscillatory motion in a side-heated cavity. *J. Fluid Mech.*, **213**, 589–610

Schladow, S. G., Patterson, J. C., and Street, R. L. 1989. Transient flow in a side-heated cavity at high Rayleigh number: a numerical study. *J. Fluid Mech.*, **200**, 121–148

Weaver, J. A. and Viskanta, R. 1990. Comparison of predicted and measured three-dimensional natural convection in a rectangular box. *Fundamentals of Natural Convection*, V. S. Arpaci and Y. Bayazitoglu (Eds.). *ASME HTD*, **140**, 113–122

Winters, K. H. 1987. Hopf bifurcation in the double-glazing problem with conducting boundaries. *J. Heat Transfer*, **109**, 894–898

Yang, H. Q., Yang, K. T., and Xia, Q. 1989. Periodic laminar convection in a tall vertical cavity. *Int. J. Heat Mass Transfer*, **32**, 2199–2207

Yewell, R., Poulikakos, D., and Bejan, A. 1982. Transient natural convection experiments in shallow enclosures. *J. Heat Transfer*, **104**, 533–538

Zhong, Z. Y., Yang, K. T., and Lloyd, J. R. 1985. Variable property effects in laminar natural convection in a square enclosure. *J. Heat Transfer*, **107**, 133–138

Note added in proof

In a recent article (Ravi, M. R., Henkes, R. A. W. M. and Hoogendoorn, C. J. 1994. On the high-Rayleigh-number structure of steady laminar natural-convection flow in a square enclosure. *J. Fluid Mech.*, **262**, 325–351), the corner structure associated with flow separation and recirculation, which was previously considered to be an internal hydraulic jump (Ivey 1984; Lee and Kauh 1984), is ascribed to purely thermal effects. They assert that, based on arguments of mechanical energy loss at the corner, internal hydraulic jumps could not be present.